

A Physics-Informed Indirect Method for Trajectory Optimization

Kun Wang^{*1}, Fangmin Lu^{†1}, Zheng Chen^{‡1,2*} and Jun Li^{§1,2}

¹*School of Aeronautics and Astronautics, Zhejiang University, Hangzhou 310027, Zhejiang, China*

²*Huanjiang Lab, Zhuji, 311816, Zhejiang, China*

The indirect method has long been favored for solving trajectory optimization problems due to its ability to reveal the structure of the corresponding optimal control. However, providing an appropriate initial guess of the co-state vector remains challenging due to its lack of physical significance. To address this issue, this paper introduces a Physics-Informed Indirect Method (PIIM), for which all shooting variables are constrained into a narrow space by utilizing their physics information. Starting from the Time-Optimal Soft Landing Problem (TOSLP), an analytical estimation method for the minimum flight time is provided; we show that the co-state vector at the final time can be constrained on a unit 3-D hypersphere by eliminating the mass co-state and the numerical factor used in the initial co-state vector normalization; and the physical significance of the optimal control at the final time is exploited, allowing to further narrow down the solution space for the co-state vector to a unit 3-D octant sphere. Then, by incorporating the above physics-informed information into a shooting function that involves of propagating the dynamics of both states and co-states backward, the PIIM achieves faster and more robust convergence for the TOSLP compared to existing indirect methods. In addition, the combination of the PIIM with a homotopy approach is proposed, allowing one to solve the fuel-optimal soft landing problem robustly. Finally, numerical simulations are presented to demonstrate and validate the developments of the paper.

I. INTRODUCTION

A trajectory optimization problem aims to determine a sequence of inputs to a dynamical system, while satisfying specific constraints and minimizing a predefined cost function. Due to the inherent nonlinearity of many real-world applications, numerical methods are commonly employed to generate optimal trajectories. The growing interest in space exploration, coupled with advancements in digital computing, has spurred academic and industrial sectors to develop efficient numerical methods to tackle intricate technical challenges.

The first thorough classification of numerical methods for trajectory optimization was comprehensively conducted by

^{*}PhD student, School of Aeronautics and Astronautics, Student member.

[†]PhD student, School of Aeronautics and Astronautics, Student member.

[‡]Researcher, School of Aeronautics and Astronautics. email: z-chen@zju.edu.cn (Corresponding author).

[§]Professor, School of Aeronautics and Astronautics.

Betts [1], wherein direct and indirect methods were considered. The direct method transforms the trajectory optimization problem into a nonlinear programming problem via collocation methods, which is then solved by the interior-point or sequential quadratic programming methods. However, this approach often entails a large number of variables, resulting in computationally expensive solutions. On the other hand, the indirect method transforms the trajectory optimization problem into a Two-Point Boundary-Value Problem (TPBVP) based on the necessary conditions from Pontryagin's Minimum Principle (PMP). The resulting TPBVP is usually solved by the indirect shooting method based on Newton's method. Compared to the direct method, the indirect method offers two advantages. First, it reveals the structure of the optimal control through the necessary conditions. Second, it involves a smaller number of variables during the solution process, leading to faster convergence when the initial guess is sufficiently close to the optimal solution. However, the co-state vector is typically abstract with no physical significance, which makes providing an appropriate initial guess intricate and non-intuitive. Meanwhile, the indirect shooting method, when attempting to satisfy the terminal conditions, is very sensitive to the initial guess of the co-state vector [2]. Consequently, [the convergence region for the initial co-state vector is often extremely narrow](#). Albeit not suitable for onboard implementation because the resulting solution is open-loop and solved offline, the indirect method has been widely used in obtaining the nominal trajectory, crucial for generating the real-time optimal solution via neural networks [3] or polynomial map guidance [4]. Therefore, extensive efforts have been made to find appropriate initial guesses that facilitate convergence and enhance the robustness of the indirect method.

Dixon and Biggs [5] introduced the adjoint control transformation to estimate physical controls and their derivatives, thus replacing the need for the initial co-state vector. This technique significantly reduced the sensitivity for orbital transfer problems. Subsequently, this technique was extended to other applications [6–9]. Another popular approach involves directly obtaining the analytical or approximate solution for the co-state vector by solving a simplified problem. For example, in [10], an analytic co-state vector was obtained by simplifying the dynamics and disregarding the effects of the central body and mass variation. In [11], a flat Earth model with constant gravity was employed to initialize the fuel-optimal orbit transfer problem. Additionally, in [12], for an optimal control problem concerning an endoatmospheric launch vehicle, an analytical initialization was first obtained, followed by a continuation method on the system dynamics to find the optimal solution of the original system. In [13], an analytic solution to the co-state vector from a gravity-free energy-optimal control problem was utilized to find the fuel-optimal trajectory for asteroid landing. In [14], the Lambert solution with irregular gravity was used to approximate the co-state vector for a fuel-optimal descent trajectory planning problem. After obtaining the analytical solution for a simplified one-dimensional landing problem, an adaptive homotopy process was designed to link the one-dimensional problem with the three-dimensional one in [15]. By using some reduced trajectory optimization problems as transitions, some final states and the co-state vector were initialized in analytical forms for the original minimum-time low-thrust problem in [16]. In a low-thrust minimum-time station change problem [17], the tangential-thrust control was considered as the optimal control candidate, and the final

time and co-state vector were approximated. Under an assumption of constant gravitational acceleration, the concept of zero-effort-miss/zero-effort-velocity has been used to derive closed-form suboptimal solutions [18, 19]. In [20], based on analytical results of a minimum-time problem, the optimal co-states were estimated to facilitate the solving procedure for the fuel-optimal lunar ascent problem. Recently, in virtue of the Hamiltonian being a linear function of the co-state vector, the optimality conditions were transformed into linear forms of the co-state vector, and the initial co-state vector was estimated by solving a set of linear algebraic equations [21]. In addition, shape-based methods, describing the geometric shape of the trajectory using mathematical expressions with tunable parameters, have also been widely used for trajectory optimization problems [22–25]. Specifically, shape-based methods have been applied to estimate the co-state vector for low-thrust transfer problems [23–25]. Moreover, heuristic techniques have been used to initiate the co-state vector [26, 27].

In contrast to the approximation-based methods in the preceding paragraph, some works focus on reducing the solution space for the co-state vector. Lu et al. [28] analyzed a transversality condition in the optimal ascent problem and revealed that the co-state vector could be scaled by any positive constant without altering the optimal trajectory. Then, the Initial Co-state Vector Normalization (ICVN) was proposed in [29]. In this work, through multiplying the cost function by a positive unknown numerical factor, the trajectory optimization problem was homogenized w.r.t. the co-state vector, effectively constraining the initially unbounded co-state vector to lie on a unit hypersphere. While originally designed for the fuel-optimal low-thrust problem, the ICVN has been applied to time-optimal problems [30, 31].

The conventional indirect method propagates both states and co-states forward in time, which usually makes the shooting function very sensitive to the initial guess of the co-state vector. Therefore, some works have aimed to mitigate this sensitivity. For instance, [32] suggested that backward propagation could ensure the fulfillment of terminal conditions [more easily compared to the forward propagation](#). Meanwhile, some assumptions were made at the final time to reduce the solution space. In [33], a forward-backward method was proposed to divide the trajectory by an intermediate point into two segments, and the trajectory optimization problem was formulated as a multi-PBVP rather than a TPBVP. During the solving process, the trajectory before the intermediate point was propagated forward, but the trajectory after the intermediate point was propagated backward. This forward-backward process allows for reducing the sensitivities of the shooting function.

In summary, without simplifying the dynamics, the ICVN stands out as a powerful method for significantly reducing the solution space for the initial co-state vector down to a unit hypersphere. However, confining the initial co-state vector to remain on the unit hypersphere may not always guarantee a very high convergence rate, as will be shown in Section VI. Additionally, backward propagation of the dynamics is able to facilitate convergence of the shooting function because the terminal conditions can be fulfilled more easily. Despite this potential, the benefits of backward propagating the dynamics have not been extensively explored.

On the other hand, continuation or homotopy methods have been frequently embedded into the indirect method to facilitate convergence [11–13, 29, 30, 33–36]. When solving the fuel-optimal problem, a more straightforward subproblem, usually the energy-optimal problem, is often formulated within the continuation framework [29, 34, 37]. However, the significance of the energy-optimal problem is probably limited to initializing the fuel-optimal problem because the thrust magnitude in the energy-optimal problem is continuously changing, potentially rendering it infeasible for spacecraft operations. In contrast, the time-optimal solution provides the minimum flight time for any feasible trajectory [38]. Therefore, it is natural to investigate the direct connection between the time- and fuel-optimal problems.

Due to these reasons, in this paper we propose a Physics-Informed Indirect Method (PIIM) to efficiently and robustly solve two commonly studied trajectory optimization problems: the Time-Optimal Soft Landing Problem (TOSLP) and the Fuel-Optimal Soft Landing Problem (FOSLP). **The key of the PIIM is that it provides all shooting variables, including the minimum flight time and unknown co-states, with physics-informed information.** For the TOSLP, unlike the approach to generate the minimum flight time iteratively by combining extrapolation and bisection methods [38], we provide an accurate estimation of the minimum flight time. We then show that the mass co-state and the numerical factor used in the ICVN can be eliminated by analyzing the dynamics at the final time. In contrast to existing works [32, 33], one of the highlights of the PIIM is that, by propagating the dynamics of both states and co-states backward, it leverages the physical significance of the co-state vector at the final time to narrow down its solution space. In this way, **all the physics-informed information is embedded into a shooting function formulated within the framework of the PIIM.** Consequently, the solution space for all shooting variables can be reduced, allowing to facilitate convergence and improve the robustness of the indirect method. We summarize the main contributions of the paper as follows:

- 1) We show that the co-state vector at the final time can be constrained on a unit 3-D hypersphere by eliminating the mass co-state and the numerical factor for the TOSLP.
- 2) The physical significance of the optimal control at the final time is exploited, allowing to narrow down the solution space for the co-state vector at the final time to a unit 3-D octant sphere. Then, the PIIM can be implemented by incorporating the above physics-informed information into a shooting function that involves of propagating the dynamics of both states and co-states backward.
- 3) We find that the final time tends to converge to a negative value if the initial guess of the co-state vector is not accurate enough. Thus, a simple remedy strategy is proposed to guarantee that the final time remains positive in the shooting procedure.
- 4) A direct connection between the TOSLP and the FOSLP is established by combining the PIIM-based TOSLP with a homotopy approach, allowing to solve the FOSLP more quickly and robustly.

The structure of this paper is as follows. Section II presents statements for the TOSLP and FOSLP. **In Section III, the conventional indirect method based on the ICVN is briefly introduced.** The PIIM for the TOSLP is detailed in Section IV. Section V outlines the conventional approach and the homotopy approach proposed to solve the FOSLP. In Section

VI, we present numerical simulations to demonstrate benefits of the proposed method. Section VII concludes the paper.

II. PROBLEM FORMULATION

Consider the planar motion of a lunar lander described in Fig. 1. Assume that the Moon is a regular spherical body

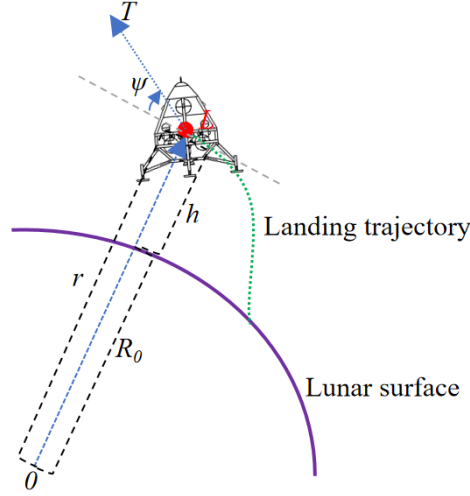


Fig. 1 Coordinate system for the lunar soft landing.

and the influences of the Moon's rotation can be neglected. The origin O is fixed at the Moon's center. Denote by $r \geq R_0$ (R_0 is the radius of the Moon) the radial distance between the origin O and the lunar lander L , thus the altitude of the lunar lander can be expressed as $h = r - R_0$. The lunar lander is propelled by an engine, whose thrust magnitude and thrust steering angle are adjustable. The thrust magnitude is denoted by $T \in [0, T_m]$, where the constant T_m means the maximum thrust magnitude. Let $u \in [0, 1]$ denote the engine thrust ratio, then we have $T = uT_m$. The thrust steering angle, denoted by $\psi \in [-\frac{\pi}{2}, \frac{\pi}{2}]$, is defined to be the angle from the local horizontal line to the thrust vector. It is worth mentioning that since the landing site is not fixed, the optimal trajectory is rotatable. Therefore, the initial range angle of the lunar lander, i.e., its initial angle information in the coordinate system, does not influence the solution. Then, the point-mass dynamics of the lunar lander can be described by [39]

$$\begin{cases} \dot{r}(t) = v(t), \\ \dot{v}(t) = u(t)T_m \sin \psi(t)/m(t) - \mu/r^2(t) + r(t)\omega^2(t), \\ \dot{\omega}(t) = -[u(t)T_m \cos \psi(t)/m(t) + 2v(t)\omega(t)]/r(t), \\ \dot{m}(t) = -u(t)T_m/(I_{sp}g_e), \end{cases} \quad (1)$$

where $t \geq 0$ is the time, the over dot denotes the differentiation w.r.t. time, v is the speed along the direction of OL , i.e., the radial speed, and ω represents the angular velocity. Thus, the transverse speed is given by ωr . μ represents the gravitational constant of the Moon, and m is the mass of the lunar lander. The constant I_{sp} denotes the specific impulse of the lunar lander's propulsion system, while g_e represents the Earth's gravitational acceleration at sea level. The initial condition of the lunar lander at time $t_0 = 0$ is specified by

$$r(0) = r_0, v(0) = v_0, \omega(0) = \omega_0, m(0) = m_0. \quad (2)$$

It is evident that at touchdown, we have $r(t_f) = R_0$ (t_f is the free final time). Meanwhile, we expect to have zero speed at touchdown, namely $v(t_f) = 0$ and $\omega(t_f) = 0$. Hence, the terminal condition can be expressed as

$$r(t_f) = R_0, v(t_f) = 0, \omega(t_f) = 0. \quad (3)$$

To improve numerical conditioning, we use $R_0, \sqrt{\frac{\mu}{R_0}}, m_0, \sqrt{\frac{R_0^3}{\mu}}$, and $\frac{m_0 \mu}{R_0^2}$ to normalize r, v, m, t , and T_m , respectively. Note that μ will be normalized to 1. To avoid abuse of notation, we continue to use the same notation as in (1) for the dimensionless counterpart hereafter.

To address the TOSLP, it amounts to finding control variables $u(t), \psi(t)$, and the final time t_f , to steer the dynamical system in (1) from the initial condition in (2) to the terminal condition in (3), such that the cost function,

$$J_T = \int_0^{t_f} 1 dt, \quad (4)$$

is minimized, where the subscript T is used in the context of TOSLP when necessary.

Unlike the TOSLP, the FOSLP minimizes the following cost function:

$$J_F = \int_0^{t_f} u dt, \quad (5)$$

where the subscript F is used in the context of FOSLP when necessary.

III. CONVENTIONAL INDIRECT METHOD FOR THE TOSLP

Let $\mathbf{x} = [r, v, \omega, m]^T$ be the state vector and $\mathbf{p}_x = [p_r, p_v, p_\omega, p_m]^T$ the co-state vector. The nonlinear dynamics in (1) can be rewritten as

$$\dot{\mathbf{x}}(t) = \mathbf{f}(\mathbf{x}, u, \psi, t), \quad (6)$$

where $f : \mathbb{R}^4 \times \mathbb{R} \times \mathbb{R} \times \mathbb{R}_0^+ \rightarrow \mathbb{R}^4$ is the smooth vector field defined in (1).

Denote by $p_0 > 0$ an arbitrary positive numerical factor. The cost function in (4) is changed to

$$J_{\text{T,ICVN}} = p_0 \int_0^{t_f} 1 \, dt. \quad (7)$$

The Hamiltonian, denoted by $\mathcal{H}_{\text{T,ICVN}}$, is formulated as

$$\mathcal{H}_{\text{T,ICVN}} = p_r v + p_v \left(\frac{u T_m}{m} \sin \psi - \frac{\mu}{r^2} + r \omega^2 \right) + p_\omega \left[- \left(\frac{u T_m}{m} \cos \psi + 2v\omega \right) / r \right] + p_m \left(- \frac{u T_m}{I_{\text{sp}} g_e} \right) + p_0. \quad (8)$$

According to PMP [40], we have

$$\begin{cases} \dot{p}_r(t) = -\frac{2p_v \mu}{r^3} - p_v \omega^2 - p_\omega \left[\left(\frac{u T_m}{m} \cos \psi + 2v\omega \right) / r^2 \right], \\ \dot{p}_v(t) = -p_r + 2p_\omega \omega / r, \\ \dot{p}_\omega(t) = -2p_v r \omega + 2p_\omega v / r, \\ \dot{p}_m(t) = p_v u T_m \sin \psi / m^2 - p_\omega u T_m \cos \psi / (m^2 r). \end{cases} \quad (9)$$

Minimizing $\mathcal{H}_{\text{T,ICVN}}$ w.r.t. ψ implies

$$\begin{bmatrix} \sin \psi \\ \cos \psi \end{bmatrix} = - \frac{1}{\sqrt{p_v^2 + \left(-\frac{p_\omega}{r} \right)^2}} \begin{bmatrix} p_v \\ -\frac{p_\omega}{r} \end{bmatrix}. \quad (10)$$

For the optimal engine thrust ratio, we have

$$u(t) = \begin{cases} 1, & S(t) \leq 0 \\ 0, & S(t) > 0 \\ \text{undetermined}, & S(t) = 0 \end{cases}$$

where $S(t)$ denotes the switching function, defined as

$$S(t) = \frac{\partial \mathcal{H}_{\text{T,ICVN}}}{\partial u}. \quad (11)$$

Substituting (10) into (11) leads to

$$S(t) = -T_m \left\{ \frac{1}{m(t)} \sqrt{p_v^2(t) + \left[\frac{p_\omega(t)}{r(t)} \right]^2} + \frac{p_m(t)}{I_{sp} g_e} \right\}.$$

The free final mass of the lunar lander implies

$$p_m(t_f) = 0. \quad (12)$$

With some algebraic manipulations, it can be shown that, combining the dynamics for p_m , (10) with (12) leads to $p_m(t) > 0, \forall t \in [0, t_f]$. Therefore, we have that $S(t)$ is always negative and thus:

$$u(t) \equiv 1, \forall t \in [0, t_f]. \quad (13)$$

Because the Hamiltonian in (8) does not contain time explicitly and the final time is free, it holds that

$$\mathcal{H}_{T,ICVN}(t) \equiv 0, \forall t \in [0, t_f]. \quad (14)$$

Meanwhile, p_0 and the initial co-state vector are normalized to stay on a unit 5-D hypersphere, i.e.,

$$p_0^2 + p_{r_0}^2 + p_{v_0}^2 + p_{\omega_0}^2 + p_{m_0}^2 = 1, \quad (15)$$

which is called the *normalization condition*.

Then, the initial co-state vector and final time can be found by solving the following shooting function:

$$\Phi_T^f(z_{T,ICVN}^f) = [r(t_f) - R_0; v(t_f); \omega(t_f); p_m(t_f); p_0^2 + p_{r_0}^2 + p_{v_0}^2 + p_{\omega_0}^2 + p_{m_0}^2 - 1; \mathcal{H}_{T,ICVN}(t_f)] = \mathbf{0}, \quad (16)$$

where $z_{T,ICVN}^f = [p_{r_0}, p_{v_0}, p_{\omega_0}, p_{m_0}, p_0, t_f]^T$ is the shooting vector. The superscript f implies that the dynamics are propagated *forward*; Notice that p_0 cannot be 1, otherwise $[p_{r_0}, p_{v_0}, p_{\omega_0}, p_{m_0}]^T = \mathbf{0}$, which contradicts PMP.

Denote by t_{\max} the maximum value for the final time t_f . Since the thrust magnitude remains at its maximum during landing, t_{\max} can be given by [22] (for simplicity, we ignore the dry mass of the lunar lander)

$$t_{\max} = m_0 \frac{I_{sp} g_0}{T_m}. \quad (17)$$

Thus, the solution space for (16) becomes

$$p_{r_0} \in (-1, 1), p_{v_0} \in (-1, 1), p_{\omega_0} \in (-1, 1), p_{m_0} \in (0, 1), p_0 \in (0, 1), t_f \in (0, t_{\max}]. \quad (18)$$

IV. PIIM FOR THE TOSLP

In this section, we first provide an analytical estimation of the minimum flight time t_f . Then, we show that the mass co-state p_m can be eliminated and the numerical factor p_0 does not change the optimal solution by using a physical fact at the final time. This not only ensures that the initial co-state vector is constrained on a unit 3-D hypersphere, but also leads to the consideration of propagating the dynamics backward. The physical significance of the optimal control at the final time is exploited, allowing to narrow down the solution space. As a result, all the physics-informed information brought by the PIIM is incorporated into the shooting function.

A. Estimation of the minimum flight time

By taking the lunar surface as the zero of potential energy, the initial energy of the lunar lander, denoted by E_0 , is

$$E_0 = \frac{1}{2}m_0[v_0^2 + (\omega_0 r_0)^2] + m_0 \frac{\mu}{r_0^2}(r_0 - R_0).$$

It is clear that the energy of the lunar lander reaches zero at touchdown. Therefore, the energy variation during landing is $\Delta E = E_0 - 0 = E_0$. Denote by Δm the fuel consumption during landing, and let $\Delta \hat{m}$ be the estimation of Δm . Since the thrust is mainly used to nullify the energy of the lunar lander, according to Tsiolkovsky's rocket equation [41], the fuel consumption can be estimated by

$$\Delta \hat{m} \approx m_0 - m(t_f) \approx \eta m_0 [1 - \exp(-\frac{\Delta V}{I_{sp} g_e})], \quad (19)$$

where η is a constant, and ΔV is the change in velocity, which can be approximated by

$$\frac{1}{2}m_0 \Delta^2 V \approx \Delta E.$$

Due to the fact that the fuel consumption for finite thrust is slightly larger than that of impulsive thrust regarding the same change in velocity ΔV , we set $\eta = 1.05$. As a result, the estimation of the minimum flight time t_f , denoted by \hat{t}_f , can be given by

$$t_f \approx \hat{t}_f = \frac{\Delta \hat{m}}{|\dot{m}|} = \frac{\Delta \hat{m} I_{sp} g_e}{T_m}. \quad (20)$$

B. Elimination of the mass co-state and the numerical factor

Notice that p_m is not included in the right-hand side of (1) and (9). In addition, the optimal thrust steering angle ψ in (10) is also independent of p_m . Meanwhile, the optimal engine thrust ratio remains at its maximum regardless of p_m . Hence, its initial value p_{m_0} has no impact on the integration of the state equation in (1) and the co-state equation in (9) except for the dynamics of p_m in (9).

According to (9) and (10), the mass co-state variation, denoted by Δp_m , can be obtained by

$$\Delta p_m = p_m(t_f) - p_{m_0} = \int_0^{t_f} \dot{p}_m(t) dt = \int_0^{t_f} -\frac{uT_m}{m^2(t)} \left\{ \sqrt{p_v^2(t) + \left[\frac{p_\omega(t)}{r(t)} \right]^2} \right\} dt. \quad (21)$$

Since all the elements on the right-hand side of (21) are independent of p_{m_0} , it is evident that Δp_m is also independent of p_{m_0} . Consequently, once the terminal condition in (3) and the stationary condition in (14) are met, $p_m(t_f) = 0$ will automatically hold true by selecting $p_{m_0} = -\Delta p_m$. It is important to recall that p_0 can be any positive number without changing the nature of the optimal solution. Once the optimal solution is obtained, we set a new numerical factor, denoted by p'_0 , via multiplying p_0 by a scaling factor $k = \frac{1}{\sqrt{1-(\Delta p_m)^2}} > 1$, i.e.,

$$p'_0 = kp_0 = \frac{1}{\sqrt{1-(\Delta p_m)^2}} p_0.$$

Since the dynamics of states and co-states, as well as the optimal control equations are homogeneous to p_0 and the initial co-state vector, we have

$$p'_{r_0} = kp_{r_0}, p'_{v_0} = kp_{v_0}, p'_{\omega_0} = kp_{\omega_0},$$

where the prime indicates the solution related to the new numerical factor p'_0 . Meanwhile, along the same optimal trajectory with different numerical factors p_0 and p'_0 , the following relation holds:

$$p'_r(t'_f) = kp_r(t_f), p'_v(t'_f) = kp_v(t_f), p'_\omega(t'_f) = kp_\omega(t_f), t'_f = t_f, m'(t'_f) = m(t_f). \quad (22)$$

By substituting (3), (10), and (12), (13) into (8), and considering (14), we can deduce

$$\mathcal{H}_{\text{ICVN}}(t_f) = -\frac{T_m}{m(t_f)} \sqrt{p_v^2(t_f) + p_\omega^2(t_f)} - p_v(t_f) + p_0 = 0. \quad (23)$$

Combining (22) with (23), we immediately have

$$\mathcal{H}'_{\text{ICVN}}(t'_f) = k \left\{ -\frac{T_m}{m(t_f)} \sqrt{p_v^2(t_f) + p_\omega^2(t_f)} - p_v(t_f) + p_0 \right\},$$

which will be equal to zero once (23) is met. Additionally, in view of (15), the scaled numerical factor and initial co-state vector satisfy

$$p_0'^2 + p_{r_0}'^2 + p_{v_0}'^2 + p_{\omega_0}'^2 = k^2[1 - (\Delta p_m)^2] = 1.$$

Hence, for any p_0 , we can always set a new numerical factor $p_0' = k p_0$ such that p_{m_0} can be eliminated from the *normalization condition* in (15). To avoid notation abuse, we will still use the same notation for the scaled counterpart. Consequently, (15) becomes

$$p_0^2 + p_{r_0}^2 + p_{v_0}^2 + p_{\omega_0}^2 = 1. \quad (24)$$

Thus, (16) becomes

$$\Phi_T^f(\mathbf{z}_{\text{T,ICVN}}^f) = [r(t_f) - R_0; v(t_f); \omega(t_f); p_0^2 + p_{r_0}^2 + p_{v_0}^2 + p_{\omega_0}^2 - 1; \mathcal{H}_{\text{T,ICVN}}(t_f)] = \mathbf{0}, \quad (25)$$

where $\mathbf{z}_{\text{T,ICVN}}^f = [p_{r_0}, p_{v_0}, p_{\omega_0}, p_0, t_f]^T$ is the shooting vector independent of p_{m_0} .

Next, we shall show that p_0 does not influence the optimal solution. By [using a physical fact](#), we show that $p_0 > 0$ always holds true as long as (23) is satisfied.

Proposition 1 *For any $p_v(t_f)$ and $p_\omega(t_f)$, (23) always leads to a positive numerical factor p_0 .*

Proof. First, in order for (23) to hold true, it is necessary that $p_v(t_f)$ and $p_\omega(t_f)$ cannot both be zero. During the final phase of the landing, the thrust magnitude must be greater than the gravitational force to nullify the touchdown speed. Meanwhile, the gravitational acceleration at touchdown, i.e., $\frac{\mu}{r^2(t_f)}$ with $r(t_f) = R_0$, is normalized to 1. Therefore, we have $T_m > m(t_f)$. As a result, it is evident that

$$p_0 = \frac{T_m}{m(t_f)} \sqrt{p_v^2(t_f) + p_\omega^2(t_f)} + p_v(t_f) > 0$$

always holds true, thereby completing the proof. \square

As stated in [31], p_0 can be set to a fixed value in advance and remains unchanged during the solution process. Therefore, according to Proposition 1 and [31], (24) does not need to be satisfied, and (14) can be replaced by the following equation:

$$p_{r_0}^2 + p_{v_0}^2 + p_{\omega_0}^2 = 1, \quad (26)$$

which is called the Simplified ICVN (SICVN), as done in [31]. Then, (25) becomes

$$\Phi_T^f(\mathbf{z}_{T,\text{SICVN}}^f) = [r(t_f) - R_0; v(t_f); \omega(t_f); p_{r_0}^2 + p_{v_0}^2 + p_{\omega_0}^2 - 1] = \mathbf{0}, \quad (27)$$

in which $\mathbf{z}_{T,\text{SICVN}}^f = [p_{r_0}, p_{v_0}, p_{\omega_0}, t_f]^T$ is the shooting vector independent of p_{m_0} and p_0 . As a result, p_0 can be determined by (23) once (27) is solved. Moreover, the solution space for the co-state vector in (27) is

$$p_{r_0} \in (-1, 1), p_{v_0} \in (-1, 1), p_{\omega_0} \in (-1, 1). \quad (28)$$

C. Backward propagating of dynamics

Since the developments of the preceding subsection are derived by analyzing the dynamics at the final time, we consider propagating the dynamics backward.

Define a new time variable τ as below

$$\tau = t_f - t, t \in [0, t_f].$$

It is palpable that the dynamics can also be propagated backward in time, i.e., from $t = t_f$ to $t = 0$. In such case, the dynamics are transformed into

$$\begin{cases} \dot{\mathbf{x}}(\tau) = -\mathbf{f}(\mathbf{x}, u, \psi, \tau), \\ \dot{\mathbf{p}}_x(\tau) = \frac{\partial \mathcal{L}(\tau)}{\partial \mathbf{x}(\tau)}. \end{cases} \quad (29)$$

For the TOSLP with the same boundary conditions, the initial condition in (2) becomes the terminal condition when the dynamics are propagated backward, i.e.,

$$r(\tau)|_{\tau=t_f} = r_0, v(\tau)|_{\tau=t_f} = v_0, \omega(\tau)|_{\tau=t_f} = \omega_0, m(\tau)|_{\tau=t_f} = m_0. \quad (30)$$

Likewise, the terminal condition in (3) becomes the initial condition, i.e.,

$$r(\tau)|_{\tau=0} = R_0, v(\tau)|_{\tau=0} = 0, \omega(\tau)|_{\tau=0} = 0. \quad (31)$$

In such case, the variable τ represents the *time of flight*. Note that the optimal control equations for the dynamical system in (29) remain the same as in (10) and (13) once the variable t is replaced by τ .

To propagate the dynamics in (29) from $\tau = 0$ to $\tau = t_f$, we need the unknown initial state $m(\tau)|_{\tau=0}$ and initial

co-state vector $\mathbf{p}_x(\tau)|_{\tau=0} = [p_r(\tau), p_v(\tau), p_\omega(\tau)]^T|_{\tau=0}$. Notably, $p_m(\tau)|_{\tau=0}$ is eliminated because it does not alter the propagation on the remaining states and co-states. Given (31), $m(\tau)|_{\tau=0}$ and $\mathbf{p}_x(\tau)|_{\tau=0}$ to be determined, the final states and co-states can be calculated through integrating (29) along with the optimal control equations. Notice that along the optimal trajectory, $\mathcal{H}_{\text{T,ICVN}}(t) \equiv 0$ holds true for $t \in [0, t_f]$. For (29), we consider the Hamiltonian $\mathcal{H}_{\text{T,ICVN}}(\tau)$ at $\tau = 0$ for the stationary condition. Recall that (26) can replace the stationary condition. Thus, the TOSLP is transformed into a new TPBVP, which seeks to find $m(\tau)|_{\tau=0}$, $\mathbf{p}_x(\tau)|_{\tau=0}$, and t_f such that (30) and (31) are satisfied, i.e.,

$$\Phi_T^b(\mathbf{z}_{\text{T,ICVN}}^b) = [r(\tau)|_{\tau=t_f} - r_0; v(\tau)|_{\tau=t_f} - v_0; \omega(\tau)|_{\tau=t_f} - \omega_0; m(\tau)|_{\tau=t_f} - m_0; p_r^2(\tau) + p_v^2(\tau) + p_\omega^2(\tau)|_{\tau=0} - 1] = \mathbf{0}, \quad (32)$$

where the superscript b denotes the *backward* propagation, and the shooting vector $\mathbf{z}_{\text{T,ICVN}}^b$ is

$$\mathbf{z}_{\text{T,ICVN}}^b = [p_r(\tau), p_v(\tau), p_\omega(\tau), m(\tau), t_f]^T|_{\tau=0}. \quad (33)$$

Compared with (27), $\mathbf{z}_{\text{T,ICVN}}^b$ has one more unknown variable $m(\tau)|_{\tau=0}$, which is related to the fuel consumption during landing. Fortunately, $m(\tau)|_{\tau=0}$ can be obtained by $m(\tau)|_{\tau=0} = m_0 - \Delta m$ according to (19). In the next subsection, we focus on reducing the solution space for $[p_r(\tau), p_v(\tau), p_\omega(\tau)]^T|_{\tau=0}$.

D. Reducing the solution space by exploiting the optimal control

Notice that the solution space for the co-state vector in (33) is constrained on a unit 3-D hypersphere. In what follows, we shall show that the solution space can be further reduced to a unit 3-D octant sphere.

Proposition 2 *Let a short time interval $t \in [t_f - t_1, t_f]$ (t_1 is a small positive number) denote the final phase of the landing until touchdown. It holds true that $p_v(\tau) < 0$ and $p_\omega(\tau) > 0$ for the interval $\tau = t_f - t \in (0, t_1]$.*

Proof. For the interval $t \in [t_f - t_1, t_f]$, in view of (1), the radial distance $r(t)$ will monotonically decrease to R_0 , indicating that $\dot{r}(t) < 0$, which further implies that $v(t) < 0$. To nullify the radial speed at touchdown, it is necessary to have $\dot{v}(t) > 0$. Moreover, since the angular velocity $\omega(t)$ is very close to zero in such an interval, the second equation in (1) becomes

$$\dot{v}(t) \approx \frac{T_m}{m(t)} \sin \psi(t) - \frac{\mu}{r^2(t)} > 0.$$

Since $r(t) \approx 1$ for $t \in [t_f - t_1, t_f]$ and the estimation of $m(t)$, denoted by $\hat{m}(t)$, can be obtained by (19), we have

$$\sin \psi(t) > \frac{\hat{m}(t)}{T_m}. \quad (34)$$

Analogously, to nullify the angular velocity at touchdown, $\omega(t)$ should gradually decrease to zero, yielding $\dot{\omega}(t) < 0$. In view of the fourth equation in (1), we have

$$\cos \psi(t) > 0. \quad (35)$$

Combining (34) with (35), it is obvious that

$$\arcsin \frac{\hat{m}(t)}{T_m} < \psi(t) < \frac{\pi}{2}. \quad (36)$$

Using the optimal thrust steering angle in (10) infers that $p_v(t) < 0$ and $p_w(t) > 0$, $t \in [t_f - t_1, t_f)$, indicating that

$$p_v(\tau) < 0 \text{ and } p_w(\tau) > 0, \tau \in (0, t_1], \quad (37)$$

which completes the proof. \square

Next, let us analyze the solution space for $p_r(\tau)|_{\tau=0}$. In view of (10), by differentiating $\sin \psi$ w.r.t τ , along with some algebraic manipulations, we obtain

$$\dot{\psi}(\tau) \cos \psi(\tau)|_{\tau=0} = \frac{p_r(\tau)p_\omega^2(\tau)}{[p_v^2(\tau) + p_\omega^2(\tau)]^{\frac{3}{2}}}|_{\tau=0}. \quad (38)$$

Combining the second equation in (10) with (38) leads to

$$\dot{\psi}(\tau)|_{\tau=0} = \frac{p_r(\tau)p_\omega(\tau)}{p_v^2(\tau) + p_\omega^2(\tau)}|_{\tau=0}. \quad (39)$$

Since the thrust steering angle defines the body attitude of the lunar lander [42], it is desirable to ensure that the thrust steering angle at touchdown is such that the lunar lander has a vertical attitude. If not, a terminal descent phase is usually needed to ensure a vertical landing. In such case, to ensure a smooth and gentle landing, it is reasonable to assume that the thrust steering angle gradually increases towards 90 deg, or at least tends to do so until touchdown. In other words, we have $\dot{\psi}(t) > 0$ for $t \in [t_f - t_1, t_f]$, which is equivalent to $\dot{\psi}(\tau) > 0$ for $\tau \in [0, t_1]$. Therefore, in view of (37) and (39), we obtain

$$p_r(\tau)|_{\tau=0} > 0. \quad (40)$$

So far, according to (37) and (40), the solution space has been further reduced to

$$p_r(\tau)|_{\tau=0} \in (0, 1), p_v(\tau)|_{\tau=0} \in (-1, 0), p_\omega(\tau)|_{\tau=0} \in (0, 1). \quad (41)$$

In the next section, to demonstrate the developments of the PIIM, we shall first present the conventional indirect method to solve the FOSLP by adopting the ICVN. Then, we will combine the PIIM with a homotopy approach to directly connect the TOSLP and the FOSLP.

V. PROCEDURES FOR SOLVING THE FOSLP

A. Conventional indirect method using the ICVN

By introducing an arbitrary positive numerical factor p_{0F} , the cost function in (5) is changed to

$$J_{F,ICVN} = p_{0F} \int_0^{t_f} u \, dt. \quad (42)$$

The Hamiltonian, denoted by $\mathcal{H}_{F,ICVN}$, is reconstructed as

$$\mathcal{H}_{F,ICVN} = p_r v + p_v \left(\frac{u T_m}{m} \sin \psi - \frac{\mu}{r^2} + r \omega^2 \right) + p_\omega \left[- \left(\frac{u T_m}{m} \cos \psi + 2v\omega \right) / r \right] + p_m \left(- \frac{u T_m}{I_{sp} g_e} \right) + p_{0F} u.$$

Equations (1), (9), and (10) still hold true, expect that the optimal engine thrust ratio $u_F(t)$ becomes

$$u_F(t) = \begin{cases} 1, & S_F(t) \leq 0 \\ 0, & S_F(t) > 0 \end{cases}$$

where $S_F(t)$ is the switching function satisfying

$$S_F(t) = p_{0F} - T_m \left\{ \frac{1}{m(t)} \sqrt{p_v^2(t) + \left[\frac{p_\omega(t)}{r(t)} \right]^2} + \frac{p_m(t)}{I_{sp} g_e} \right\}.$$

Since $u_F(t)$ is bang-bang, which may result in numerical difficulties, we adopt the smoothing technique from [43] to approximate $u_F(t)$, i.e.,

$$u_F(t) \approx u_F(t, \delta) = \frac{1}{2} \left(1 - \frac{S_F(t)}{\sqrt{|S_F(t)|^2 + \delta}} \right), \quad (43)$$

in which δ is a small positive constant.

Meanwhile, we have the following *normalization condition*:

$$p_{0F}^2 + p_{r_0}^2 + p_{v_0}^2 + p_{\omega_0}^2 + p_{m_0}^2 = 1. \quad (44)$$

The shooting function is

$$\Phi_F^f(\mathbf{z}_{\text{F,ICVN}}^f(\delta)) = [r(t_f) - R_0; v(t_f); \omega(t_f); p_m(t_f); p_{0F}^2 + p_{r_0}^2 + p_{v_0}^2 + p_{\omega_0}^2 + p_{m_0}^2 - 1; \mathcal{H}_{\text{F,ICVN}}(t_f)] = \mathbf{0}, \quad (45)$$

where $\mathbf{z}_{\text{F,ICVN}}^f(\delta) = [p_{r_0}, p_{v_0}, p_{\omega_0}, p_{m_0}, p_{0F}, t_f]^T$. Since the lower bound for the thrust magnitude is zero, according to (20), the solution space for (45) is

$$p_{r_0} \in (-1, 1), p_{v_0} \in (-1, 1), p_{\omega_0} \in (-1, 1), p_{m_0} \in (0, 1), p_{0F} \in (0, 1), t_f \in [\hat{t}_f, +\infty). \quad (46)$$

B. Homotopy approach

Since the PIIM can reduce the solution space down to be sufficiently small for the TOSLP, it is natural to directly connect the TOSLP with the FOSLP within the homotopy framework. Denote by κ a homotopy parameter that connects (7) with (5), i.e.,

$$J_h = \int_0^{t_f} p_0 \kappa + (1 - \kappa) u \, dt, \quad (47)$$

where the subscript h denotes the context of *homotopy*. It can be observed that J_h becomes $J_{\text{T,ICVN}} = \int_0^{t_f} p_0 \, dt$ in (7) if $\kappa = 1$. On the other hand, J_h becomes $J_F = \int_0^{t_f} u \, dt$ in (5) if $\kappa = 0$. In this manner, the TOSLP serves as the seeding problem, whose solution can be found using the PIIM developed in Section IV. Then, by decreasing κ from 1 to 0, the homotopy process can be completed by using the preceding convergent solution as the initial guess. Next, we shall present the corresponding shooting functions during the homotopy process.

Notice that the dynamical model and boundary conditions remain the same as in Section II. Considering the cost function in (47), the Hamiltonian is

$$\mathcal{H}_h(\kappa) = p_0 \kappa + (1 - \kappa) u + p_r v + p_v \left(\frac{u T_m}{m} \sin \psi - \frac{\mu}{r^2} + r \omega^2 \right) + p_\omega \left[- \left(\frac{u T_m}{m} \cos \psi + 2v\omega \right) / r \right] + p_m \left(- \frac{u T_m}{I_{\text{sp}} g_e} \right).$$

Therefore, (9) and (10) still hold true. Since the optimal engine thrust ratio $u_h(\tau, \kappa)$ is linear w.r.t. the state dynamics

and cost function, it is reasonable to assume that $u_h(\tau, \kappa)$ is bang-bang, i.e.,

$$u_h(\tau, \kappa) = \begin{cases} 1, & S_h(\tau, \kappa) \leq 0 \\ 0, & S_h(\tau, \kappa) > 0 \end{cases}$$

where $S_h(\tau, \kappa)$ is the switching function satisfying

$$S_h(\tau, \kappa) = -T_m \left\{ \frac{1}{m(\tau)} \sqrt{p_v^2(\tau) + \left[\frac{p_\omega(\tau)}{r(\tau)} \right]^2} + \frac{p_m(\tau)}{I_{sp} g_e} \right\} + 1 - \kappa.$$

Once again, the smoothing technique from [43] is used to approximate $u_h(\tau, \kappa)$, i.e.,

$$u_h(\tau, \kappa) \approx u_h(\tau, \kappa, \delta) = \frac{1}{2} \left(1 - \frac{S_h(\tau)}{\sqrt{|S_h(\tau)|^2 + \delta}} \right), \quad (48)$$

in which δ is the same constant as in (43).

The corresponding TPBVP amounts to solving the following shooting function:

$$\Phi_h^b(z_{h,\text{SICVN}}^b(\kappa, \delta)) = [r(\tau, \kappa, \delta) - r_0; v(\tau, \kappa, \delta) - v_0; \omega(\tau, \kappa, \delta) - \omega_0; m(\tau, \kappa, \delta) - m_0; \mathcal{H}_h(\tau, \kappa, \delta)]|_{\tau=t_f} = \mathbf{0}, \quad (49)$$

where $z_{h,\text{SICVN}}^b(\kappa, \delta) = [p_r(\tau, \kappa, \delta), p_v(\tau, \kappa, \delta), p_\omega(\tau, \kappa, \delta),$

$m(\tau, \kappa, \delta), t_f(\kappa, \delta)]^T|_{\tau=0}$. It is important to note that, unlike the TOSLP where p_m is not needed, the dynamics of p_m must be included here because the switching function is related to p_m . When propagating the dynamics of p_m , it is clear that its initial value is $p_m(\tau)|_{\tau=0} = 0$.

Keep in mind that (32) is equivalent to (49) when $\kappa = 1$. In such case, the smoothing constant δ does not change the optimal thrust magnitude because it will remain at the maximum; meanwhile, the last equation in (32) is used to replace the stationary condition, i.e., the last equation in (49). Instead of finding the solution to the FOSLP by directly solving (45), we shall present a homotopy process, as stated in Fig. 2, to solve the FOSLP through starting with the PIIM-based TOSLP. In Fig. 2, i and j are the updating indices for the homotopy parameters κ and δ , respectively. The parameter n is the backtracking number for solving (49). This means that if the shooting function does not converge even after adopting the homotopy parameter updating procedure 5 times, the algorithm fails.

VI. NUMERICAL SIMULATIONS

This section presents some simulations to showcase the developments in Sections IV and V. Before proceeding, we shall define some constants. The propulsion system of the lunar lander is specified by $I_{sp} = 300$ s and $T_m = 1,500$ N. The radius of the Moon is $R_0 = 1,738$ km, and g_e is 9.81 m/s². Additionally, the gravitational constant μ is

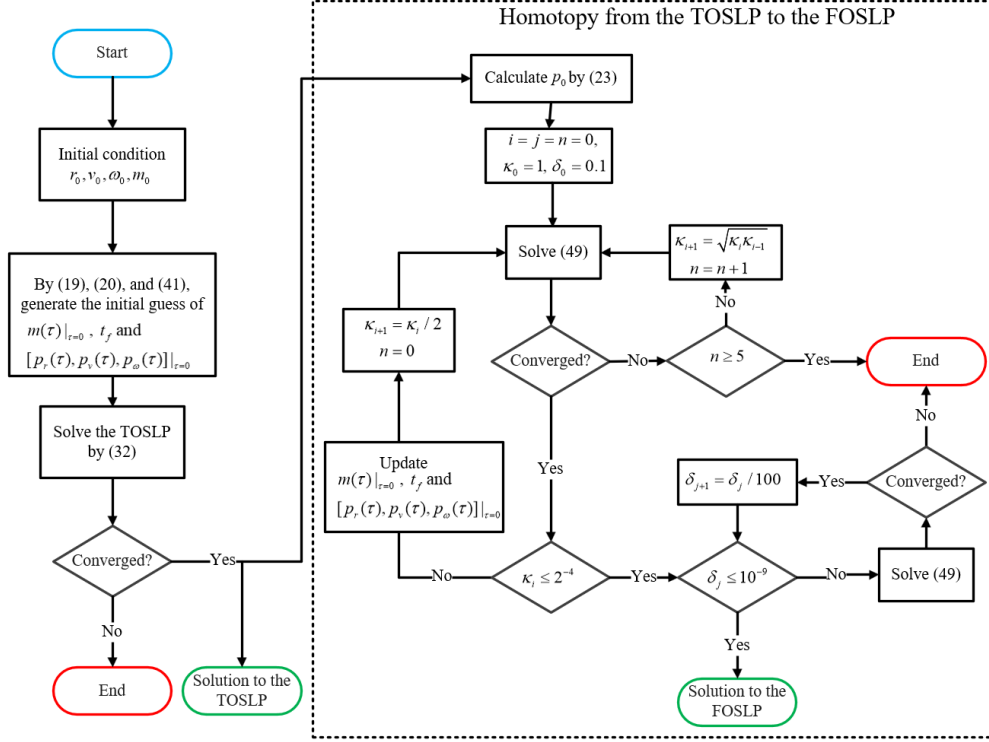


Fig. 2 Flowchart for solving the TOSLP and using its solution to solve the FOSLP via the homotopy process.

$4.90275 \times 10^{12} \text{ m}^3/\text{s}^2$. All the algorithms are implemented on a desktop equipped with an AMD EPYC 9684X 96-Core Processor @2.55 GHz and 128 GB of RAM. The absolute and relative tolerances for propagating the dynamics are set as 1.0×10^{-9} . The nonlinear equation solver *fsolve* is used to find the zero of the shooting function. The termination tolerance and maximum number of iterations for *fsolve* are set as 1.0×10^{-9} and 300, respectively.

A. Simulations on the TOSLP

To assess the convergence and robustness of the proposed method, a total of 10,000 initial conditions are randomly generated in a domain $\mathcal{A} := \{(r_0, v_0, \omega_0, m_0) \mid r_0 \in [1738, 1911.9738] \text{ km}, v_0 \in [-83.9779, 83.9779] \text{ m/s}, \omega_0 \in [0, 9.6638 \times 10^{-4}] \text{ rad/s}, m_0 \in [240, 600] \text{ kg}\}$.

1. Efficacy of Subsection IV.A in Section IV

Here we demonstrate the significance of the analytical estimation of the minimum flight time in (20). Equation (16) is solved for these initial conditions. The corresponding shooting vector is initialized by randomly generating numbers in the specified domain in (18). On the other hand, we initialize the minimum flight time according to (20). Notice that, for a fair comparison, each initial condition among the 10,000 cases remains the same.

Table 1 summarizes the numerical results in terms of some important indicators. To be specific, the successful landing means that not only the shooting function is solved successfully, but also the resulting trajectory is physically

Table 1 Quantitative comparison of the results by solving $\Phi_T^f(z_{T,ICVN}^f)$ in (16) using different initial guesses for t_f

Item	$t_f \in (0, t_{\max}]$	$t_f = \hat{t}_f$
No. of successful landings	5,501	6,757
No. of convergent solutions with $t_f < 0$	2,705	2,677
No. of convergent solutions with $r(t) < R_0$	80	75
Average computational time (s)	0.2463	0.1062
Average No. of iterations	24.87	21.54
Average No. of function evaluations	154.83	131.79

feasible, i.e., $t_f > 0$ and the radial distance $r(t) \geq R_0$ for $t \in [0, t_f]$. Clearly, providing the analytical estimation of the minimum flight time can improve the success rate for finding the optimal feasible trajectory. Regarding the average computational time, which is calculated as the sum of computational times for successful landings divided by the number of successful landings, initializing $t_f = \hat{t}_f$ reduces the average computational time from 0.2463 seconds to 0.1062 seconds. Therefore, we only compare the results obtained by initializing the minimum flight time according to (20) hereafter.

2. Efficacy of Subsections IV.B-IV.D in Section IV

We further solve another two shooting functions in (27) and (32) for these initial conditions. The corresponding shooting vector is initialized according to (28) and (41), respectively. Table 2 summarizes the numerical results. Compared with the indirect methods that propagate the dynamics forward, i.e., solving $\Phi_T^f(z_{T,ICVN}^f)$ and $\Phi_T^f(z_{T,SICVN}^f)$, solving $\Phi_T^b(z_{T,SICVN}^b)$ on the basis of the PIIM presents the highest success rate for finding the optimal feasible trajectory. Although many solutions are convergent, the resulting final times are negative for $\Phi_T^f(z_{T,ICVN}^f)$ and $\Phi_T^f(z_{T,SICVN}^f)$, as indicated by 2,677 and 3,591 cases. This is because these two shooting functions have a larger solution space than the PIIM-based shooting function. This fact will increase the likelihood of generating a wrong initial guess that leads to the nonlinear function solver converging to a solution with $t_f < 0$.

Table 2 Quantitative comparison of the results by solving different shooting functions

Item	$\Phi_T^f(z_{T,SICVN}^f)$ in (27)	$\Phi_T^b(z_{T,SICVN}^b)$ in (32)
No. of successful landings	5,731	9,887
No. of convergent solutions with $t_f < 0$	3,591	42
No. of convergent solutions with $r(t) < R_0$	92	48
Average computational time (s)	0.0831	0.0613
Average No. of iterations	30.79	13.49
Average No. of function evaluations	128.46	68.58

Table 3 Quantitative comparison of the results after using the remedy strategy

Item	$\Phi_T^f(z_{T,ICVN}^f)$ in (16)	$\Phi_T^f(z_{T,SICVN}^f)$ in (27)	$\Phi_T^b(z_{T,SICVN}^b)$ in (32)
No. of successful landings	9,928	9,930	9,952
No. of convergent solutions with $t_f < 0$	0	0	0
No. of convergent solutions with $r(t) < R_0$	48	48	48
Average computational time (s)	0.0903	0.0955	0.0557
Average No. of iterations	16.53	34.87	11.21
Average No. of function evaluations	102.69	148.00	58.71
Success rate (%)	99.76	99.78	100

Furthermore, these three shooting functions result in 75, 92, and 48 cases of convergent but infeasible solutions with $r(t) < R_0$ (indicating that the lunar lander is flying underneath the lunar surface), respectively. For the average computational time, solving $\Phi_T^b(z_{T,SICVN}^b)$ in (32) requires the shortest time compared to other two. Meanwhile, the numbers of iterations and function evaluations are also the lowest among the three.

3. A remedy strategy ensuring $t_f > 0$

Notice that the initial guess of the minimum flight time remains the same for all three shooting functions, so it is reasonable to conclude that providing an inappropriate initial guess of the co-state vector increases the likelihood of converging to an infeasible solution with a negative final time, as indicated by the numbers of convergent solutions with $t_f < 0$ in Table 2. To resolve this issue, a simple remedy strategy is proposed here.

The variable t_f in the shooting function is first replaced by a new variable ξ . Then the integration interval is changed from $[0, t_f]$ to $[0, \exp(\xi)]$. This ensures that the iteration of the final time will remain positive. It should be noted that the initial guess of ξ is given by $\log(\hat{t}_f)$, where \hat{t}_f is calculated according to (20).

With the remedy strategy, we run another test for the same 10,000 cases. The numerical results are displayed in Table 3, from which we can see that, the numbers of successful landings are improved for the three shooting functions. The reported numbers of convergent solutions with $t_f < 0$ are all reduced to zero as expected. Meanwhile, they share the same number of convergent solutions with $r(t) < R_0$, which is 48 out of 10,000 cases. Since the initial condition is randomly generated in \mathcal{A} , it is possible that the initial condition does not have a solution inherently. For the 48 cases, we find that $r(t) < R_0$ holds for all obtained solutions despite trying a large number of initial guesses, so it is reasonable to conclude that these cases do not have feasible solutions. In such case, we can see that solving $\Phi_T^b(z_{T,SICVN}^b)$ in (32) exhibits a success rate of 100%. In contrast, solving $\Phi_T^f(z_{T,ICVN}^f)$ and $\Phi_T^f(z_{T,SICVN}^f)$ results in a success rate of 99.76% and 99.78%, respectively. Moreover, after implementing the remedy strategy, the performance of solving $\Phi_T^b(z_{T,SICVN}^b)$ is further improved and outperforms the other two shooting functions, as indicated by the average computational time, number of iterations and function evaluations in Table 3. Through solving $\Phi_T^b(z_{T,SICVN}^b)$, the average computational

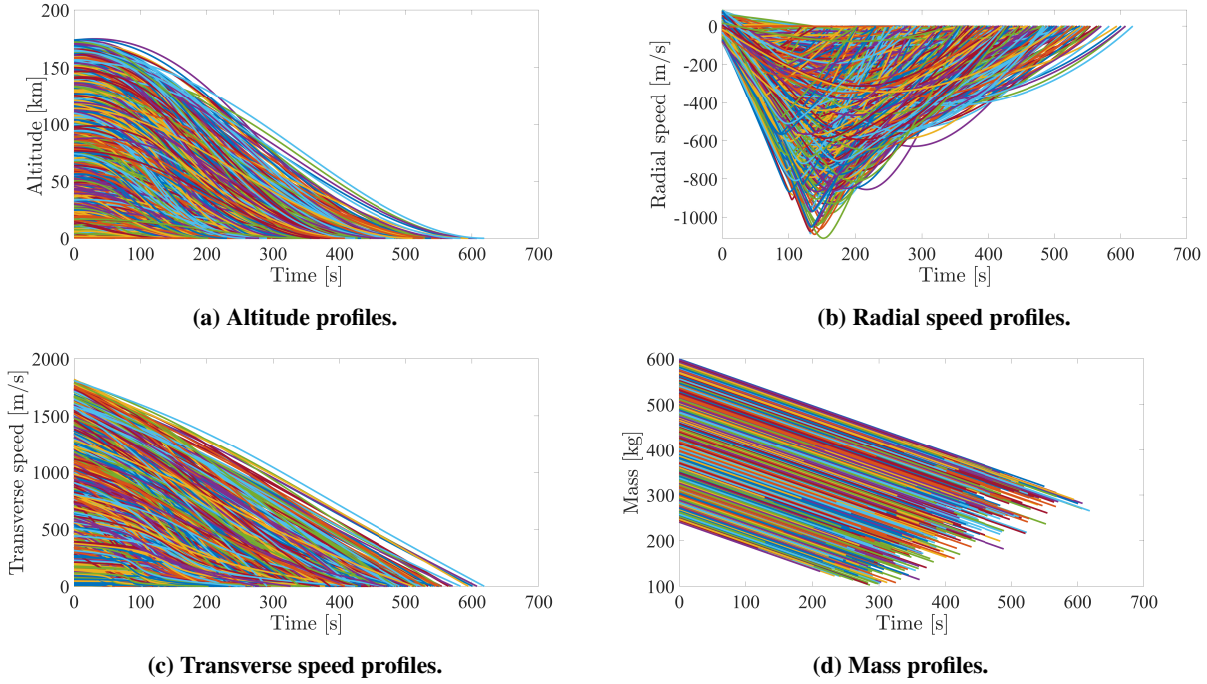


Fig. 3 Profiles of the altitude, radial speed, transverse speed, and mass.

time is decreased by 38.32% and 41.68% compared with $\Phi_T^f(z_{T,ICVN}^f)$ and $\Phi_T^f(z_{T,SICVN}^f)$, respectively. Surprisingly, although there are two less unknown variables in $\Phi_T^f(z_{T,SICVN}^f)$ than that in $\Phi_T^f(z_{T,ICVN}^f)$, the solving performance is not necessarily improved in terms of the success rate and the average computational time. More importantly, compared with a computational time of nearly 1 second in [44] where an implicit shooting method was proposed, it only takes 0.0557 seconds to find the optimal solution by solving $\Phi_T^b(z_{T,SICVN}^b)$. Thanks to the PIIM, the computational time and success rate of solving the TOSLP are improved by 77.39% and 44.72%, respectively over the conventional indirect method in Section III, as shown by the results in Tables 1 and 3.

Out of the 9,952 successful landing cases, a total of 1,000 landings are displayed in Fig. 3 in terms of altitude, radial speed, transverse speed, and mass. Although the initial condition is randomly generated, solving $\Phi_T^b(z_{T,SICVN}^b)$ can always find the optimal solution in a fast and reliable manner. To further validate the initial guess of $p_r(\tau)|_{\tau=0}$, $p_v(\tau)|_{\tau=0}$, and $p_\omega(\tau)|_{\tau=0}$ defined in (41), the convergent solutions to $p_r(\tau)|_{\tau=0}$, $p_v(\tau)|_{\tau=0}$, and $p_\omega(\tau)|_{\tau=0}$ for the 9,952 successful landing cases are shown in Figs. 4 and 5. It can be observed that $p_r(\tau)|_{\tau=0} > 0$ holds true as expected by (40). Meanwhile, (37) can also be validated, as shown by Fig. 5, in which $p_r(\tau)|_{\tau=0}$, $p_v(\tau)|_{\tau=0}$, and $p_\omega(\tau)|_{\tau=0}$ are constrained on a unit 3-D octant sphere.

B. Simulations on the FOSLP

In the preceding subsection, we demonstrated that fast and robust convergence can be achieved for the TOSLP by solving $\Phi_T^b(z_{T,SICVN}^b)$. Now, we will show that the developments of the PIIM for solving the TOSLP, can also be applied

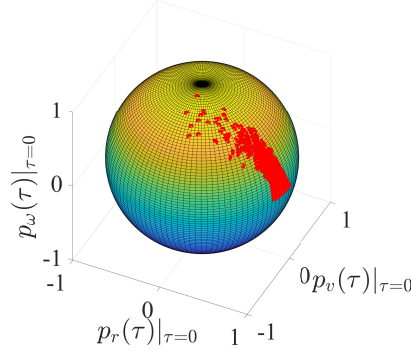


Fig. 4 Distribution of $p_r(\tau)|_{\tau=0}$, $p_v(\tau)|_{\tau=0}$, and $p_\omega(\tau)|_{\tau=0}$.

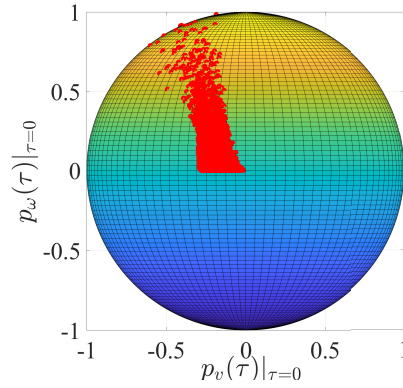


Fig. 5 Distribution of $p_v(\tau)|_{\tau=0}$ and $p_\omega(\tau)|_{\tau=0}$.

to facilitate convergence of the FOSLP.

To illustrate the homotopy process, the following initial condition is considered: $r_0 = 1,902.1754$ km, $v_0 = 23.1290$ m/s, $\omega_0 = 2.3261 \times 10^{-4}$ rad/s, and $m_0 = 483.4040$ kg. By solving (32) for the TOSLP, p_0 is found to be 0.5693, which will be used and kept unchanged in (47) throughout the homotopy process. Fig. 6 plots the homotopy path of $t_f(\kappa)$, which shows the profile of the convergent solution to the optimal final time t_f as the homotopy parameter κ is decreased from 1 to 0. During the solution process, we observe that very small values of κ may impair convergence. Thus, the homotopy process for κ is terminated once κ is decreased to a number less than 2^{-4} . It is worth mentioning that δ is kept as 0.1 before the homotopy process for κ is completed. From Fig. 6, the homotopy path turns out to be continuous and unidirectional, which makes the homotopy process straightforward [45].

The optimal thrust magnitude and thrust steering angle profiles are displayed in Figs. 7 and 8, respectively. The solution with $\kappa = 1$ represents the optimal solution to the TOSLP. Once κ is reduced below 2^{-4} , the homotopy process for δ commences. Figs. 9 and 10 illustrate the optimal thrust magnitude and thrust steering angle profiles as the smoothing constant δ decreases from 0.1 to 10^{-9} . It can be observed that while the intermediate thrust magnitude profiles are continuous, the final thrust magnitude profile with $\delta = 10^{-9}$ exhibits a bang-bang solution with a single switch. To

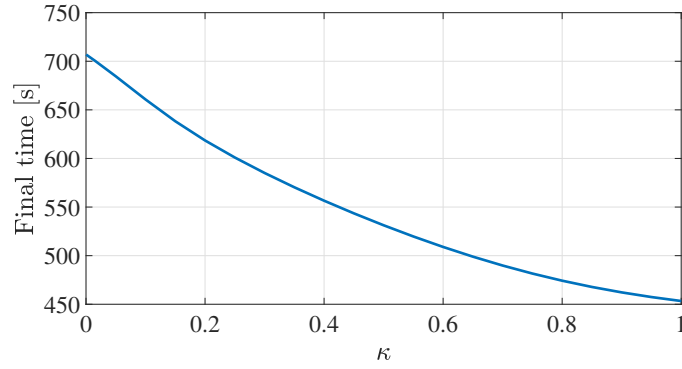


Fig. 6 Homotopy path for $t_f(\kappa)$ with $\delta = 0.1$.

provide a comprehensive analysis, the optimal altitude and mass profiles related to the TOSLP and the FOSLP are shown in Figs. 11 and 12, respectively.

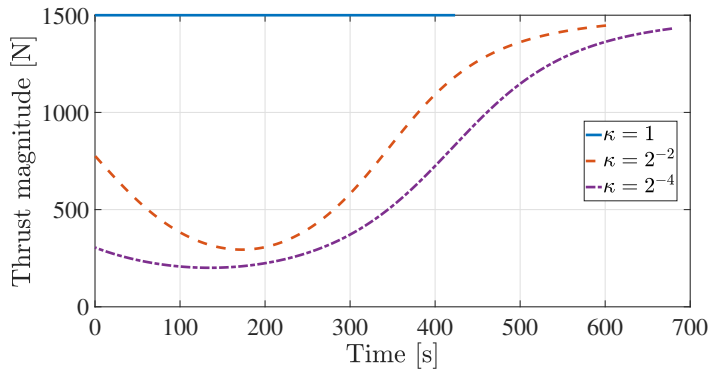


Fig. 7 Thrust magnitude profiles with different κ .

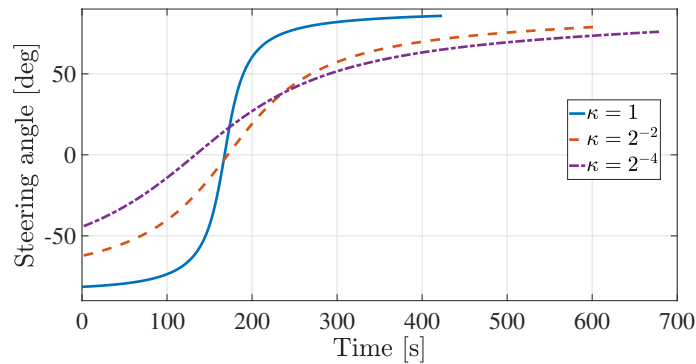


Fig. 8 Thrust steering angle profiles with different κ .

To be specific, the minimum flight time is determined to be 423.483 seconds with a fuel consumption of 215.842

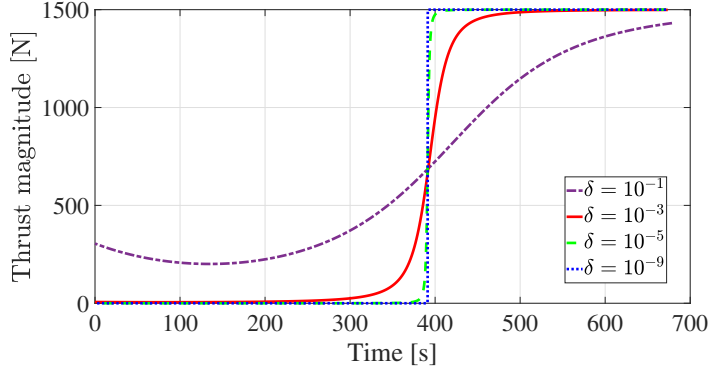


Fig. 9 Thrust magnitude profiles with different δ and $\kappa = 2^{-4}$.

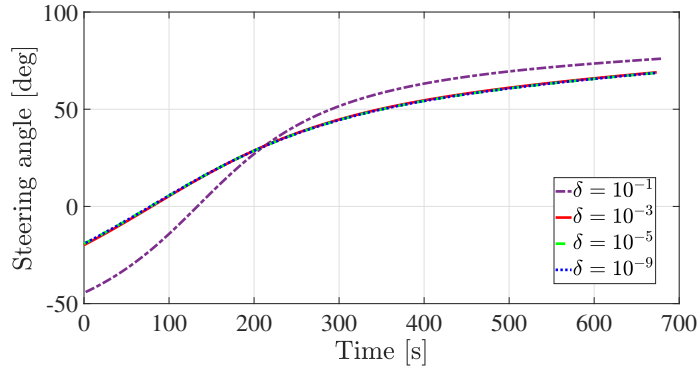


Fig. 10 Thrust steering angle profiles with different δ and $\kappa = 2^{-4}$.

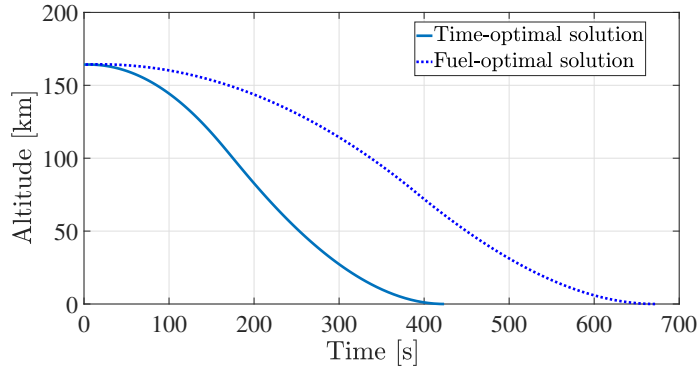


Fig. 11 Altitude profiles for the TOSLP and the FOSLP.

kg, and the thrust magnitude is kept at the maximum during landing. On the other hand, the final time for the FOSLP is 671.638 seconds with a fuel consumption of 142.905 kg, and the thrust magnitude is a typical “off-on” form. For comparison, we utilize the conventional indirect method, which resolves $\Phi_F^f(z_{F,ICVN}^f(\delta))$, to determine the optimal fuel consumption. With the same smoothing constant $\delta = 10^{-9}$, the fuel consumption derived from $\Phi_F^f(z_{F,ICVN}^f(\delta))$ is found

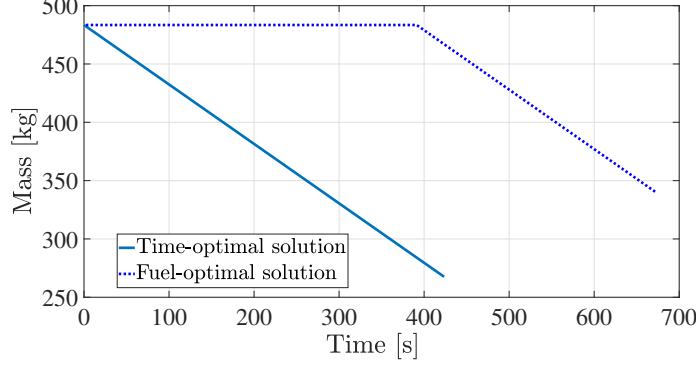


Fig. 12 Mass profiles for the TOSLP and the FOSLP.

to be 142.900 kg, which indicates that the homotopy parameter $\kappa = 2^{-4}$ incurs only a negligible penalty of 0.005 kg.

To illustrate the robustness, we compare the homotopy approach established in Fig. 2 with the conventional method by directly solving (45), in which the initial guess of the shooting vector is generated according to (46) and the final time t_f is initialized according to (20). The 9,952 successful landing cases from the preceding subsection are tested. According to [38], if the TOSLP has a feasible optimal solution, the FOSLP is also feasible under the same initial condition.

To further demonstrate the advantages of propagating the dynamics backward, we consider the same homotopy method as in (49) to solve the FOSLP except that the dynamics are propagated forward. Notice that the solution to (27) can also be used to solve the FOSLP via a homotopy approach. In such case, the dynamics of both states and co-states are propagated forward, and the shooting function in (49) becomes

$$\Phi_h^f(z_{h,SICVN}^f(\kappa, \delta)) = [r(\kappa, \delta) - R_0; v(\kappa, \delta); \omega(\kappa, \delta); p_m(\kappa, \delta); \mathcal{H}_h(\kappa, \delta)]|_{t_f} = \mathbf{0}, \quad (50)$$

where $z_{h,SICVN}^f(\kappa, \delta) = [p_{r_0}(\kappa, \delta), p_{v_0}(\kappa, \delta), p_{\omega_0}(\kappa, \delta), p_{m_0}(\kappa, \delta), t_f(\kappa, \delta)]^T$. Once the solution to (27) is obtained, the similar process in Fig. 2 is implemented. The solutions to the 9,930 successful landings obtained by solving (27) are employed to solve (50). It is worth noting that the value for p_{m_0} is obtained according to (21).

Table 4 presents the results obtained for the FOSLP using different strategies. A total of 9,952 feasible fuel-optimal solutions are found using the homotopy approach in (49), indicating a success rate of 100%. In contrast, the conventional way only finds 8,892 feasible solutions, and 57 convergent solutions are infeasible, indicated by $r(t) < R_0$. This discrepancy is likely due to poor initial guess of the shooting vector in (46). Consequently, the conventional indirect method achieves a success rate of 89.35%. Keep in mind that implementing the homotopy approach in (49) requires finding the solution to the TOSLP first, which has an average computational time of 0.0557 seconds. Therefore, for a feasible initial condition, the homotopy approach in (49) can find the fuel-optimal solution within a total computational

Table 4 Quantitative comparison of the results by solving different shooting functions

Item	$\Phi_F^f(z_{F,ICVN}^f(\delta))$ in (45)	$\Phi_h^b(z_{h,SICVN}^b(\kappa, \delta))$ in (49)	$\Phi_h^f(z_{h,SICVN}^f(\kappa, \delta))$ in (50)
No. of successful landings	8, 892	9, 952	9, 930
No. of convergent solutions with $r(t) < R_0$	57	0	0
Average computational time (s)	0.7125	0.6218	0.8348
Average No. of iterations	36.63	30.84	32.32
Average No. of function evaluations	262.97	238.72	241.59
Success rate (%)	89.35	100	99.78

time of 0.6775 seconds, which is even faster than the conventional indirect method (0.7125 seconds) despite an extra homotopy parameter κ . Remarkably, this computational efficiency is comparable to the learning-based method in [46]. Moreover, we can observe that 9, 930 feasible fuel-optimal solutions are obtained by solving (50), which is expected because the 9, 930 feasible time-optimal solutions found by solving (27) can provide accurate initialization of the shooting vector for (50). In summary, solving (50), in which the dynamics are propagated forward, requires a total computational time of 0.9303 seconds to find the solution to the TOSLP. In contrast, our proposed method decreases the average total computational time by 27.17%.

VII. CONCLUSIONS

In this work, we introduced a novel approach called Physics-Informed Indirect Method (PIIM) to solve trajectory optimization problems quickly and robustly. Its key feature is the incorporation of physics-informed information into all shooting variables. An analytical method was provided to estimate the minimum flight time. By eliminating the mass co-state and the numerical factor using a physical fact at the final time, the co-state vector at the final time was constrained on a unit 3-D hypersphere. By further propagating the dynamics backward, the physical significance of the optimal control was exploited to reduce the solution space. All the physics-informed information was embedded into a shooting function, enabling the Time-Optimal Soft Landing Problem (TOSLP) to be solved quickly and robustly. Furthermore, the PIIM was applied to a Fuel-Optimal Soft Landing Problem (FOSLP) via a homotopy approach.

Numerical simulations demonstrated that the proposed estimation of the minimum flight time improved the convergence rate, and it reduced the computational time by 56.88% to solve the TOSLP. To ensure that the final time of the convergent solution is positive, we proposed a simple remedy strategy. In this way, the computational time by using the PIIM to solve the TOSLP was reduced to 0.0557 seconds with a success rate of 100%, compared to 0.2463 seconds with a success rate of 55.28% by using the conventional indirect method. The results obtained by the homotopy approach showed that the FOSLP could be solved more quickly and robustly, which was identified by a computational time of 0.6775 seconds with a success rate of 100%, compared to 0.7125 seconds with a success rate of 89.35% by using the conventional indirect method.

Future research directions include the generalization of the PIIM to time- and fuel-optimal problems, as well as its applicability to facilitating the dataset generation for training neural networks in order to derive the real-time optimal solution.

VIII. ACKNOWLEDGMENT

The authors are grateful to Roberto Armellin, Adam Evans, and the reviewers for their valuable suggestions on improving the paper.

References

- [1] Betts, J. T., “Survey of numerical methods for trajectory optimization,” Journal of Guidance, Control, and Dynamics, Vol. 21, No. 2, 1998, pp. 193–207. <https://doi.org/10.2514/2.4231>.
- [2] Conway, B. A., “A survey of methods available for the numerical optimization of continuous dynamic systems,” Journal of Optimization Theory and Applications, Vol. 152, 2012, pp. 271–306. <https://doi.org/10.1007/s10957-011-9918-z>.
- [3] Wang, K., Lu, F., Chen, Z., and Li, J., “Real-time optimal control for attitude-constrained solar sailcrafts via neural networks,” Acta Astronautica, Vol. 216, 2024, pp. 446–458. <https://doi.org/10.1016/j.actaastro.2024.01.026>.
- [4] Evans, A., Armellin, R., Pirovano, L., and Baresi, N., “High-Order Guidance for Time-Optimal Low-Thrust Trajectories with Accuracy Control,” Journal of Guidance, Control, and Dynamics, Vol. 47, No. 2, 2024, pp. 279–290. <https://doi.org/10.2514/1.G007540>.
- [5] Dixon, L. C. W., and Biggs, M., “The advantages of adjoint-control transformations when determining optimal trajectories by Pontryagin’s Maximum Principle,” The Aeronautical Journal, Vol. 76, No. 735, 1972, pp. 169–174. <https://doi.org/10.1017/S0001924000042731>.
- [6] Kluever, C. A., and Pierson, B. L., “Optimal Earth-moon trajectories using nuclear electric propulsion,” Journal of Guidance, Control, and Dynamics, Vol. 20, No. 2, 1997, pp. 239–245. <https://doi.org/10.2514/2.4058>.
- [7] Yan, H., and Wu, H., “Initial adjoint-variable guess technique and its application in optimal orbital transfer,” Journal of Guidance, Control, and Dynamics, Vol. 22, No. 3, 1999, pp. 490–492. <https://doi.org/10.2514/2.7631>.
- [8] Ranieri, C. L., and Ocampo, C. A., “Optimization of roundtrip, time-constrained, finite burn trajectories via an indirect method,” Journal of Guidance, Control, and Dynamics, Vol. 28, No. 2, 2005, pp. 306–314. <https://doi.org/10.2514/1.5540>.
- [9] Russell, R. P., “Primer vector theory applied to global low-thrust trade studies,” Journal of Guidance, Control, and Dynamics, Vol. 30, No. 2, 2007, pp. 460–472. <https://doi.org/10.2514/1.22984>.
- [10] Thorne, J. D., and Hall, C. D., “Approximate initial Lagrange costates for continuous-thrust spacecraft,” Journal of Guidance, Control, and Dynamics, Vol. 19, No. 2, 1996, pp. 283–288. <https://doi.org/10.2514/3.21616>.

- [11] Cerf, M., Haberkorn, T., and Trélat, E., “Continuation from a flat to a round Earth model in the coplanar orbit transfer problem,” Optimal Control Applications and Methods, Vol. 33, No. 6, 2012, pp. 654–675. <https://doi.org/10.1002/oca.1016>.
- [12] Bonalli, R., Hérisse, B., and Trélat, E., “Analytical initialization of a continuation-based indirect method for optimal control of endo-atmospheric launch vehicle systems,” IFAC-PapersOnLine, Vol. 50, No. 1, 2017, pp. 482–487. <https://doi.org/10.1016/j.ifacol.2017.08.095>.
- [13] Yang, H., Li, S., and Bai, X., “Fast homotopy method for asteroid landing trajectory optimization using approximate initial costates,” Journal of Guidance, Control, and Dynamics, Vol. 42, No. 3, 2019, pp. 585–597. <https://doi.org/10.2514/1.G003414>.
- [14] Yang, H., and Li, S., “Fuel-optimal asteroid descent trajectory planning using a Lambert solution-based costate initialization,” IEEE Transactions on Aerospace and Electronic Systems, Vol. 56, No. 6, 2020, pp. 4338–4352. <https://doi.org/10.1109/TAES.2020.2988625>.
- [15] Cheng, L., Shi, P., Gong, S., and Wang, Z., “Real-time trajectory optimization for powered planetary landings based on analytical shooting equations,” Chinese Journal of Aeronautics, Vol. 35, No. 7, 2022, pp. 91–99. <https://doi.org/10.1016/j.cja.2021.07.024>.
- [16] Wu, D., Wang, W., Jiang, F., and Li, J., “Minimum-time low-thrust many-revolution geocentric trajectories with analytical costates initialization,” Aerospace Science and Technology, Vol. 119, 2021, p. 107146. <https://doi.org/10.1016/j.ast.2021.107146>.
- [17] Zhao, S., Gurfil, P., and Zhang, J., “Initial costates for low-thrust minimum-time station change of geostationary satellites,” Journal of Guidance, Control, and Dynamics, Vol. 39, No. 12, 2016, pp. 2746–2756. <https://doi.org/10.2514/1.G000431>.
- [18] Guo, Y., Hawkins, M., and Wie, B., “Applications of generalized zero-effort-miss/zero-effort-velocity feedback guidance algorithm,” Journal of Guidance, Control, and Dynamics, Vol. 36, No. 3, 2013, pp. 810–820. <https://doi.org/10.2514/1.58099>.
- [19] Wang, P., Guo, Y., Ma, G., and Wie, B., “Two-phase zero-effort-miss/zero-effort-velocity guidance for Mars landing,” Journal of Guidance, Control, and Dynamics, Vol. 44, No. 1, 2021, pp. 75–87. <https://doi.org/10.2514/1.G005242>.
- [20] Zhang, Z., Gong, S., and Li, J., “The fuel-optimal trajectory for finite-thrust LUNAR ASCENT,” Aerospace Science and Technology, Vol. 39, 2014, pp. 675–684. <https://doi.org/10.1016/j.ast.2014.06.011>.
- [21] Wu, D., Cheng, L., Jiang, F., and Li, J., “Analytical costate estimation by a reference trajectory-based least-squares method,” Journal of Guidance, Control, and Dynamics, Vol. 45, No. 8, 2022, pp. 1529–1537. <https://doi.org/10.2514/1.G006502>.
- [22] Lunghi, P., Lavagna, M., and Armellin, R., “A semi-analytical guidance algorithm for autonomous landing,” Advances in Space Research, Vol. 55, No. 11, 2015, pp. 2719–2738. <https://doi.org/10.1016/j.asr.2015.02.022>.
- [23] Taheri, E., Li, N. I., and Kolmanovsky, I., “Co-state initialization for the minimum-time low-thrust trajectory optimization,” Advances in Space Research, Vol. 59, No. 9, 2017, pp. 2360–2373. <https://doi.org/10.1016/j.asr.2017.02.010>.
- [24] Jiang, F., Tang, G., and Li, J., “Improving low-thrust trajectory optimization by adjoint estimation with shape-based path,” Journal of Guidance, Control, and Dynamics, Vol. 40, No. 12, 2017, pp. 3282–3289. <https://doi.org/10.2514/1.G002803>.

- [25] Huo, M., et al., “Fast costate estimation for indirect trajectory optimization using Bézier-curve-based shaping approach,” Aerospace Science and Technology, Vol. 126, 2022, p. 107582. <https://doi.org/10.1016/j.ast.2022.107582>.
- [26] Pontani, M., and Conway, B., “Optimal low-thrust orbital maneuvers via indirect swarming method,” Journal of Optimization Theory and Applications, Vol. 162, 2014, pp. 272–292. <https://doi.org/10.1007/s10957-013-0471-9>.
- [27] Hecht, G. R., and Botta, E. M., “Particle Swarm Optimization-based co-state initialization for low-thrust minimum-fuel trajectory optimization,” Acta Astronautica, Vol. 211, 2023, pp. 416–430. <https://doi.org/10.1016/j.actaastro.2023.06.021>.
- [28] Lu, P., Griffin, B. J., Dukeman, G. A., and Chavez, F. R., “Rapid optimal multiburn ascent planning and guidance,” Journal of Guidance, Control, and Dynamics, Vol. 31, No. 6, 2008, pp. 1656–1664. <https://doi.org/10.2514/1.36084>.
- [29] Jiang, F., Baoyin, H., and Li, J., “Practical techniques for low-thrust trajectory optimization with homotopic approach,” Journal of Guidance, Control, and Dynamics, Vol. 35, No. 1, 2012, pp. 245–258. <https://doi.org/10.2514/1.52476>.
- [30] Wijayatunga, M. C., Armellin, R., and Pirovano, L., “Exploiting scaling constants to facilitate the convergence of indirect trajectory optimization methods,” Journal of Guidance, Control, and Dynamics, Vol. 46, No. 5, 2023, pp. 958–969. <https://doi.org/10.2514/1.G007091>.
- [31] Guo, X., Wu, D., and Jiang, F., “Minimum-Time Rendezvous via Simplified Initial Costate Normalization and Auxiliary Orbital Transfer,” Journal of Guidance, Control, and Dynamics, Vol. 46, No. 8, 2023, pp. 1627–1636. <https://doi.org/10.2514/1.G007268>.
- [32] Daniel, P. P., and Epenoy, R., “Fuel optimization for low-thrust Earth–Moon transfer via indirect optimal control,” Celestial Mechanics and Dynamical Astronomy, Vol. 130, 2018, pp. 1–29. <https://doi.org/10.1007/s10569-017-9808-2>.
- [33] Sidhoum, Y., and Oguri, K., “Indirect Forward-Backward Shooting for Low-thrust Trajectory Optimization in Complex Dynamics,” AAS/AIAA Space Flight Mechanics Meeting, 2023, p. 20.
- [34] Tang, G., Jiang, F., and Li, J., “Fuel-optimal low-thrust trajectory optimization using indirect method and successive convex programming,” IEEE Transactions on Aerospace and Electronic Systems, Vol. 54, No. 4, 2018, pp. 2053–2066. <https://doi.org/10.1109/TAES.2018.2803558>.
- [35] Li, T., Wang, Z., and Zhang, Y., “A homotopy approach connecting time-optimal with fuel-optimal trajectories,” Astrophysics and Space Science, Vol. 366, 2021, pp. 1–9. <https://doi.org/10.1007/s10509-020-03890-7>.
- [36] Wang, Y., and Topputo, F., “Indirect optimization of fuel-optimal many-revolution low-thrust transfers with eclipses,” IEEE Transactions on Aerospace and Electronic Systems, Vol. 59, No. 1, 2022, pp. 39–51. <https://doi.org/10.1109/TAES.2022.3189330>.
- [37] Guo, X., Wu, D., and Jiang, F., “Multi-Phase Homotopic Approaches for Best Solution to Low-Thrust Geocentric Trajectories,” IEEE Transactions on Aerospace and Electronic Systems, 2024, pp. 1–14. <https://doi.org/10.1109/TAES.2024.3370499>, early access.

- [38] Yang, H., Bai, X., and Baoyin, H., “Rapid generation of time-optimal trajectories for asteroid landing via convex optimization,” Journal of Guidance, Control, and Dynamics, Vol. 40, No. 3, 2017, pp. 628–641. <https://doi.org/10.2514/1.G002170>.
- [39] Liu, X., Duan, G., and Teo, K. L., “Optimal soft landing control for moon lander,” Automatica, Vol. 44, No. 4, 2008, pp. 1097–1103. <https://doi.org/10.1016/j.automatica.2007.08.021>.
- [40] Pontryagin, L. S., Mathematical theory of optimal processes, Routledge, Evanston, IL, USA, 2018. <https://doi.org/10.1201/9780203749319>.
- [41] Burleson, D., “Konstantin Tsiolkovsky-The father of astronautics and rocket dynamics,” 40th AIAA Aerospace Sciences Meeting & Exhibit, 2002, p. 312. <https://doi.org/10.2514/6.2002-312>.
- [42] Lu, P., and Callan, R., “Propellant-Optimal Powered Descent Guidance Revisited,” Journal of Guidance, Control, and Dynamics, Vol. 46, No. 2, 2023, pp. 215–230. <https://doi.org/10.2514/1.G007214>.
- [43] Wang, K., Chen, Z., Wei, Z., Lu, F., and Li, J., “A New Smoothing Technique for Bang-Bang Optimal Control Problems,” AIAA SCITECH 2024 Forum, 2024, p. 0727. <https://doi.org/10.2514/6.2024-0727>.
- [44] Peng, K., Peng, R., Huang, Z., and Zhang, B., “Implicit shooting method to solve optimal Lunar soft landing trajectory,” Acta Aeronautica et Astronautica Sinica, Vol. 40, No. 7, 2019, pp. 159–167. <https://doi.org/10.7527/S1000-6893.2018.22641>.
- [45] Pan, B., Lu, P., Pan, X., and Ma, Y., “Double-homotopy method for solving optimal control problems,” Journal of Guidance, Control, and Dynamics, Vol. 39, No. 8, 2016, pp. 1706–1720. <https://doi.org/10.2514/1.G001553>.
- [46] You, S., Wan, C., Dai, R., and Rea, J. R., “Learning-based onboard guidance for fuel-optimal powered descent,” Journal of Guidance, Control, and Dynamics, Vol. 44, No. 3, 2021, pp. 601–613. <https://doi.org/10.2514/1.G004928>.